Atmospheric
Chemistry
and Physics

Supplement of

Stratospheric ozone intrusion events and their impacts on tropospheric ozone in the Southern Hemisphere

Jesse W. Greenslade et al.

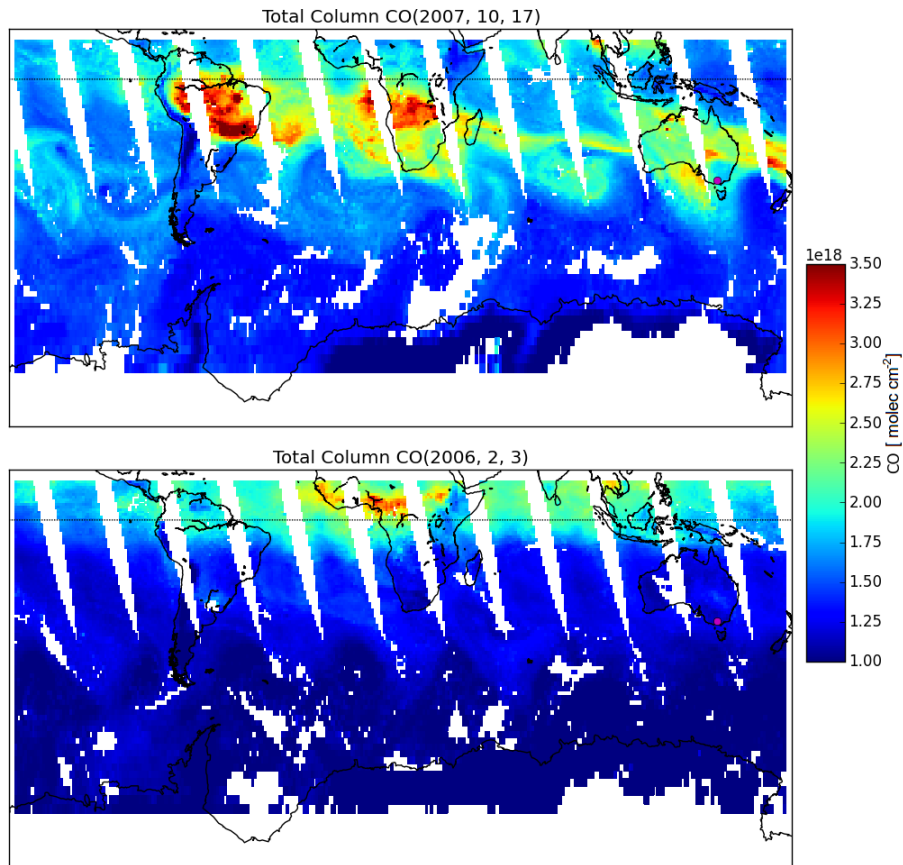*Correspondence to:* Jesse W. Greenslade (jwg366@uowmail.edu.au)

Figure S1. Example detection of biomass burning influence using AIRS total column CO. The top panel (17 October 2007) shows a day when ozone above Melbourne (purple dot) could have been caused by a transported biomass burning plume, and so was flagged in subsequent analysis. The bottom panel (3 February 2006) shows a day when ozone over Melbourne was not influenced by transported smoke.

S1 Weather and Smoke analysis

Figure S1 contrasts two days; one with and one without signs of biomass burning influence near the Melbourne site (purple circle). On 17 October 2007 (top) elevated CO suggests the site may have been influenced by long-range transport from African and/or South American biomass burning. In contrast, on 3 February 2006 (bottom) CO columns across the SH show no influence from biomass burning.

Figure S2 (left) shows the vertical ozone profile on 3 February 2005. The tropopause was between 400 and 500 hPa and ozone in the upper troposphere was anticorrelated with relative humidity, suggesting the ozone enhancements are due to dry stratospheric air. An ozone intrusion into the troposphere at $\sim$520 hPa was identified by our detection algorithm. The right panel shows the concurrent synoptic weather system, a cut-off low pressure system that caused a large storm and lowered the local tropopause height for several days. The flux of stratospheric ozone into the troposphere associated with this event,
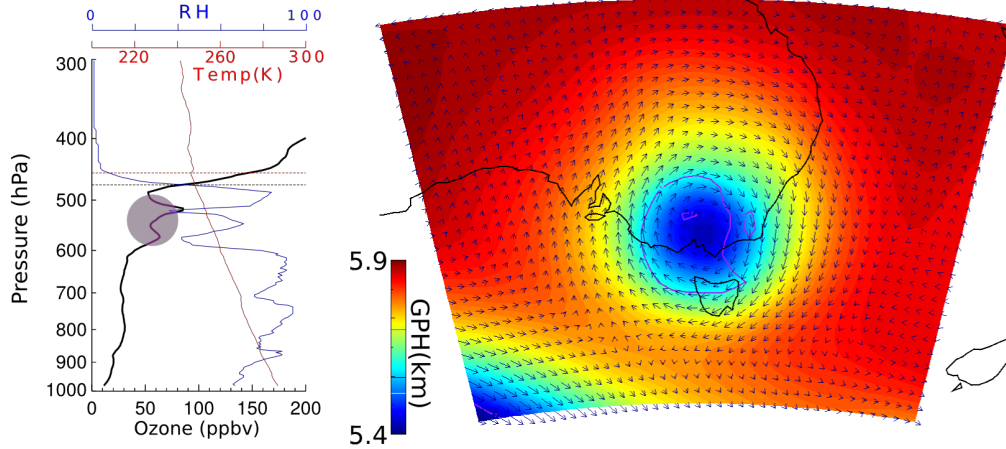
Figure S2. (Left) Vertical profile of ozone (black), relative humidity (blue), and temperature (red) measured by ozonesonde over Melbourne on 3 February 2005. The detected ozone STT event is highlighted in pink. Tropopause heights using both the ozone definition (black dashed line) and lapse rate definition (red dashed line) are also shown. (Right) Geopotential heights at 500 hPa from the ERA-Interim reanalysis, with wind vectors over-plotted. Also shown is the 1 PVU contour line (purple).

calculated using the method shown in Sect. 2.3 of the parent document, was at least 3.1×10^{11} molecules cm^{-3}, or 8% of the tropospheric ozone column.

Figure S3 (left) shows the ozone profile over Melbourne on 13 January 2010. The tropopause was higher on this date (120-160 hPa). Using our algorithm, we detected an ozone intrusion centred around 200 hPa. As before, ozone anti-correlation with relative humidity provides further evidence that the elevated ozone was stratospheric in origin. In this profile, there was clear separation between the detected intrusion (highlighted in pink) and the ozone tropopause (black dashed line), which indicates that the sonde passed through regular tropospheric air after hitting a stratospheric intrusion but before reaching the tropopause. The right panel shows that this event was associated with a trough (front) of low pressure passing over south eastern Australia. This front travelled from west to east and caused a wave of lowered tropopause height. Frontal passage is a known cause of STT as stratospheric air descends and streamers of ozone-rich air break off and mix into the troposphere (Sprenger et al., 2003).
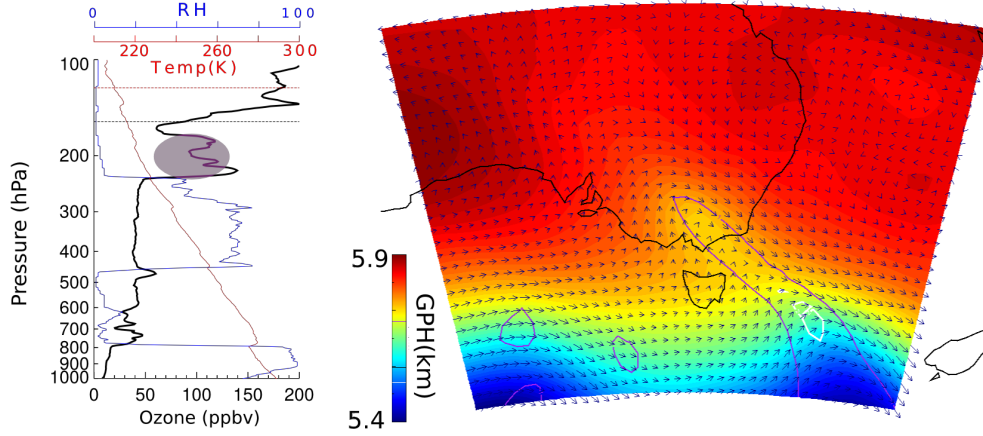
Figure S3. Same as Fig. S2 but for 13 January 2010. Also shown in this figure is the 2 PVU contour (white), often used to determine dynamical tropopause height.

S2 Southern Ocean extrapolation

S2.1 Outline

We use simulated tropospheric ozone columns from GEOS-Chem to extrapolate the ozonesonde-based estimates over a large area of the Southern Ocean encompassing our three measurement sites. Figure S4 shows the region defined by latitudes 79° - 28° S, and longitudes 53° - 175° E.

Figure S5 (upper panel) shows the factors I, P, and Ω_{O_3} which are used along with the assumed event lifetime to estimate the STT flux. The tropospheric ozone and area of our region is calculated using the output and surface area from GEOS-Chem over the Southern Ocean grid boxes along with the molecules cm^{-2} per month calculations, along with ozone molar mass of 48 g mol^{-1}.

It is worth noting that this extrapolation is very simplistic and is performed as an example of how the seasonal ozone STT calculations could be used. A more spatially resolved estimate could be determined by dividing the Southern Ocean region into longitudinal and latitudinal bins for calculating the average Ω_{O_3} from GEOS-Chem, as well as applying latitudinal gradients to P and I based on their values at the three sonde release sites, and adding longitudinal variability based on seasonal stratospheric wind jet streams (Baray et al., 2012; Škerlak et al., 2015). An improved estimate of event lifetime and parameterisation of how many events may be occuring simultaneously could also be addressed, however this is beyond the scope of this work and in any case would not address all the limitations of the estimate provided below.
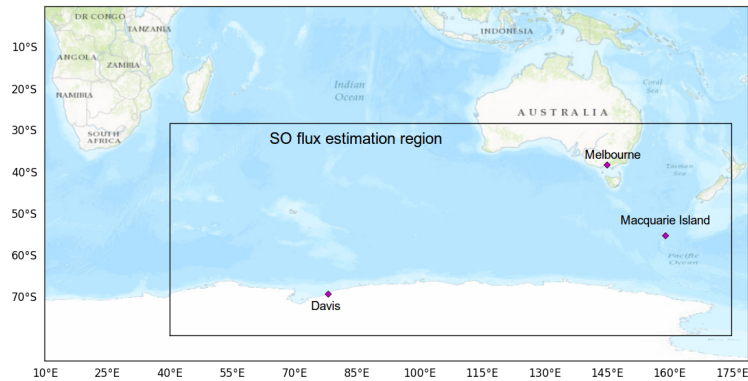
4

Figure S4. Region used for large SO estimation of STT flux

S2.2 Results

Fig. S5 (lower panel) shows the results of the calculation when we choose two days for our flux estimation, with the range
10 shown in representing the values calculated if we assume events last one day (upper bound of estimated flux) or one week
(lower bound of estimated flux). Previous studies have found STT ozone fluxes in the SH extratropics are largest from autumn
or winter to early spring (Olsen, 2003; Škerlak et al., 2015; **?**). Although these are based on dominating STT systems further
north than the area we examine here, see the main text for more details. During the SH winter, we find the highest tropospheric
Ω_{O3} but a relatively low STT flux due to reduced event frequency. Our results suggest instead that the ozone flux associated
15 with STT events (at least those due to tropopause folds) is largest in austral summer (December-March), primarily due to an
increased frequency of STT detections during these months. It is possible that our estimated event frequencies are too low in
late winter-early spring as some legitimate STT events may have been excluded due to coincident smoke plumes.

Summing the monthly estimated fluxes shown in Fig. S5 over the year, we find from this estimate that STT events may be
responsible for $\sim 7.5 \times 10^{16}$ molecules cm^{-2} yr^{-1} of the tropospheric ozone over the Southern Ocean, equivalent to 75 Tg
20 yr^{-1}. 2-16 $\times 10^{16}$ molecules cm^{-2} of stratospheric based ozone is estimated over the southern ocean throughout the year. Our
estimate is hard to directly compare to prior work that suggests global gross STT fluxes of 550 Tg yr^{-1} (Stevenson et al.,
2006) and net downward STT fluxes of 75 Tg yr^{-1} (Sprenger et al., 2003). This is due to the high uncertainties involved in
calculation as well as the specific regions which have few other measurements available.
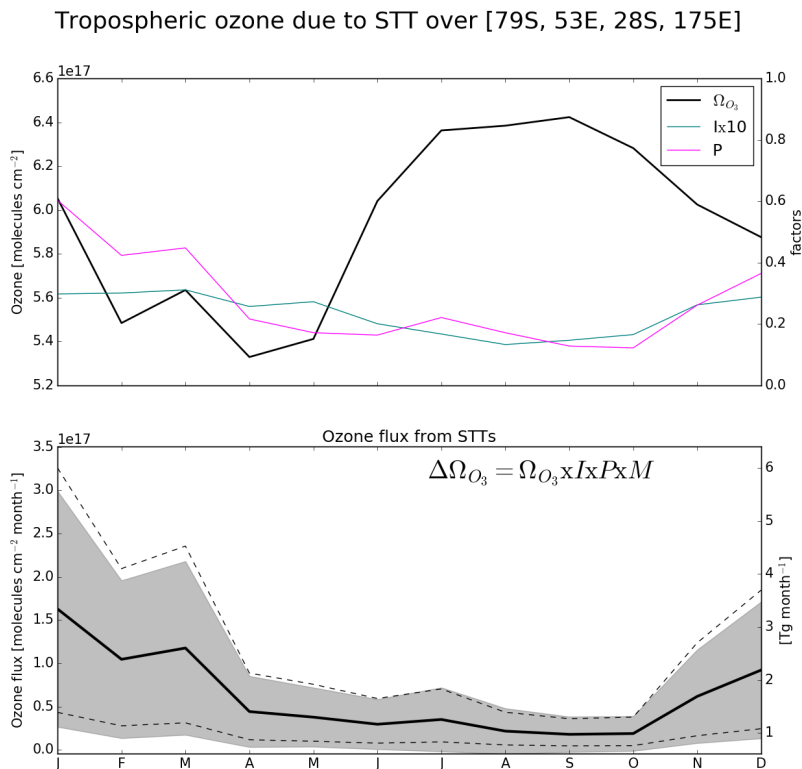
Tropospheric ozone due to STT over [79S, 53E, 28S, 175E]

Figure S5. (Top) The three quantities used to calculate the total Southern Ocean ozone flux from STT events. The tropospheric ozone column Ω_{O_3} (black, left axis) is from GEOS-Chem, while the STT probability P (magenta, right axis) and impact I (teal, right axis) are from the ozonesonde measurements. The STT impact is multiplied by 10 to better show the seasonality. (Bottom) Estimated contribution of STT to tropospheric ozone columns over the Southern Ocean. The shaded area shows the uncertainty as calculated in Sect. 6 of the parent document, with the -dashed lines showing the range of values when assuming events last one day (upper dashed line) up to one week (lower dashed line).

References

Baray, J.-L., Duflot, V., Posny, F., Cammas, J.-P., Thompson, A. M., Gabarrot, F., Bonne, J.-L., and Zeng, G.: One year ozonesonde measurements at Kerguelen Island (49.2S, 70.1E): Influence of stratosphere-to-troposphere exchange and long-range transport of biomass burning plumes, Journal of Geophysical Research, 117, doi:10.1029/2011JD016717, http://dx.doi.org/10.1029/2011JD016717, 2012.

5 Olsen, M. a.: A comparison of Northern and Southern Hemisphere cross-tropopause ozone flux, Geophysical Research Letters, 30, 1412, doi:10.1029/2002GL016538, http://doi.wiley.com/10.1029/2002GL016538, 2003.

Škerlak, B., Sprenger, M., Pfahl, S., Tyrlis, E., and Wernli, H.: Tropopause folds in ERA-Interim: Global climatology and relation to extreme weather events, Journal of Geophysical Research, 120, 4860–4877, doi:10.1002/2014JD022787, 2015.

Sprenger, M., Croci Maspoli, M., and Wernli, H.: Tropopause folds and cross-tropopause exchange: A global investigation based
10 upon ECMWF analyses for the time period March 2000 to February 2001, Journal of Geophysical Research, 108, n/a—-n/a, doi:10.1029/2002JD002587, http://dx.doi.org/10.1029/2002JD002587, 2003.

Stevenson, D. S., Dentener, F. J., Schultz, M. G., Ellingsen, K., van Noije, T. P. C., Wild, O., Zeng, G., Amann, M., Atherton, C. S., Bell, N., Bergmann, D. J., Bey, I., Butler, T., Cofala, J., Collins, W. J., Derwent, R. G., Doherty, R. M., Drevet, J., Eskes, H. J., Fiore, A. M., Gauss, M., Hauglustaine, D. A., Horowitz, L. W., Isaksen, I. S. A., Krol, M. C., Lamarque, J.-F., Lawrence, M. G., Montanaro, V., Müller, J.-F.,
15 Pitari, G., Prather, M. J., Pyle, J. A., Rast, S., Rodriguez, J. M., Sanderson, M. G., Savage, N. H., Shindell, D. T., Strahan, S. E., Sudo, K., and Szopa, S.: Multimodel ensemble simulations of present-day and near-future tropospheric ozone, Journal of Geophysical Research, 111, doi:10.1029/2005jd006338, http://dx.doi.org/10.1029/2005JD006338, 2006.